

## A new variable-mode control strategy for LLC resonant converters operating in a wide input voltage range<sup>\*</sup>

Hui-pin LIN<sup>†</sup>, Xiao-guang JIN, Liang XIE, Jin HU, Zheng-yu LU<sup>†‡</sup>

(College of Electrical Engineering, Zhejiang University, Hangzhou 310027, China)

<sup>†</sup>E-mail: linhuipin@126.com; eeluzy@cee.zju.edu.cn

Received Jan. 20, 2016; Revision accepted Nov. 10, 2016; Crosschecked Feb. 21, 2017

**Abstract:** This paper proposes a new variable-mode control strategy that is applicable for LLC resonant converters operating in a wide input voltage range. This control strategy incorporates advantages from full-bridge LLC resonant converters, half-bridge LLC resonant converters, variable-frequency control mode, and phase-shift control mode. Under this control strategy, different input voltages determine the different operating modes of the circuit. When the input voltage is very low, it works in a full-bridge circuit and variable frequency mode (FB\_VF mode). When the input voltage rises to a certain level, it shifts to a full-bridge circuit and phase-shifting control mode (FB\_PS mode). When the input voltage further increases, it shifts into a half-bridge circuit and variable frequency mode (HB\_VF mode). Such shifts are enabled by the digital signal processor (DSP), which means that no auxiliary circuit is needed, just a modification of the software. From light load to heavy load, the primary MOSFET for the LLC resonant converter can realize zero-voltage switching (ZVS), and the secondary rectifier diode can realize zero-current switching (ZCS). With an LLC resonant converter prototype with a 300 W rated power and a 450 V output voltage, as well as a resonant converter with 20–120 V input voltage, the experiments verified the proposed control strategy. Experimental results showed that under this control strategy, the maximum converter efficiency reaches 95.7% and the range of the input voltage expands threefold.

**Key words:** LLC; Full bridge; Half bridge; Variable frequency; Phase shift; Wide input voltage range  
<http://dx.doi.org/10.1631/FITEE.1600029>

**CLC number:** TM923.61

### 1 Introduction

Thanks to its environment-friendly characteristics, reliability, maturity, and cost efficiency, wind power is currently the fastest growing new energy technology. In 2012, China possessed an installed wind power capacity of 75 324 MW (Tian *et al.*, 2014), which was the highest such capacity in the world. Moreover, a 200 GW capacity in 2020 is expected (Wang *et al.*, 2013). The wind power is distributed in a wide area; however, it is distributed unevenly and changes seasonally. In light of this, the

development of wind power shows a polarized trend: (1) Large wind power plants adopt a high-capacity grid-connected wind power turbine. (2) In these distributed power generation systems (Song, *et al.*, 2003), small- and medium-sized wind power turbines prevail. Along with China's economic development, an increasing number of small- and medium-sized wind power systems are used in family and business buildings, and operated in a grid-connected manner. These facts serve as the focus in Walker and Pierce (2006).

Fig. 1 shows the structure of a distributed grid-generation system (Walker and Sernia, 2004). A wind-power generation system can be divided into several or dozens of power channels. In every one of them, the permanent magnet synchronous generator (PMSG) produces electricity (Rajaei *et al.*, 2013), the rectifier module rectifies the current (after

<sup>‡</sup> Corresponding author

<sup>\*</sup> Project supported by the National Natural Science Foundation of China (Nos. 51177148 and 51407151)

 ORCID: Zheng-yu LU, <http://orcid.org/0000-0003-1032-2938>

© Zhejiang University and Springer-Verlag Berlin Heidelberg 2017

rectification, the DC input voltage is 20–120 V), and then the DC/DC module raises the voltage to DC bus voltage (450 V). Afterwards, all the electricity in these channels gathers in a DC bus, flows through the inverter, and eventually to the grid (220 V, 50 Hz, AC, China).

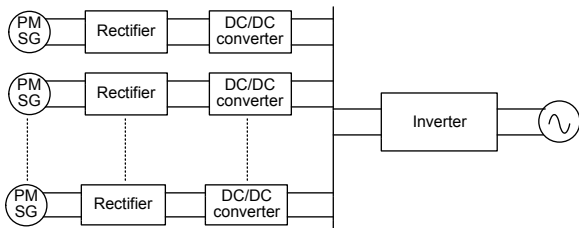


**Fig. 1 Block flow diagram of a wind power system with a DC modular grid structure (PMSG: permanent magnet synchronous generator)**

Fig. 1 indicates that due to the great disparity between input voltage (20–120 V) and output voltage (450 V) and the security regulations that must be taken into consideration, the circuit must be separated. Meanwhile, the challenge is in how to collect more energy within the super-wide input voltage range, i.e., keeping the maximum efficiency of the wind power generation system within that super-wide input range. In short, the DC/DC module has three features: (1) wider range, (2) separation, and (3) high efficiency. However, features (1) and (3) are generally contradictory.

As shown in Fig. 2, the load gain property of an LLC resonant converter is that the maximum gain increases with the load equivalent resistance, which is required by the wide input voltage range. Meanwhile, the LLC resonant converter features primary MOSFET zero-voltage switching (ZVS) and secondary diode zero-current switching (ZCS), which are the requirements for a wider range (Hu et al., 2015). Hence, the LLC resonant converter was chosen for the DC/DC module for a distributed wind power system in Jiang (2006) and Liang et al. (2010).

To maintain the high gain and wide input voltage range of the LLC resonant converter, the magnetic inductance value must be fairly low (Fang et al., 2007; Jung and Kwon, 2007; Zhang et al., 2009; Jang et al., 2012). However, the increased primary-winding MOSFET conduction loss and core loss reduce the efficiency of the LLC resonant converter (Steigerwald, 1988; Chen et al., 2010; Fang et al., 2012).

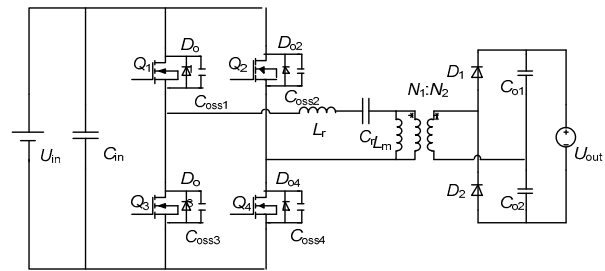


**Fig. 2 Full-bridge LLC resonant converter**

Many studies have been conducted to find ways to cope with these problems which constantly occur in traditional LLC resonant converters, and to obtain high-efficiency generation. Liang et al. (2010) proposed a mixed control strategy (Fig. 2), which doubled the DC gain by changing the full bridge into a half bridge. Nonetheless, the input voltage range of the actual wind power generation is wider; hence, such a strategy is inapplicable.

Yang et al. (2003) put forward another solution (Fig. 3) where according to the level of the input voltage, the transformation ratio was altered by shifting the secondary windings ( $W_1$  and  $W_2$ ). The problem with this structure is that it is too complex: compared to a traditional LLC resonant converter, it has one more secondary winding, two more diodes, and one more MOSFET. In other words, the circuit loss is increased, and the circuit design is difficult.

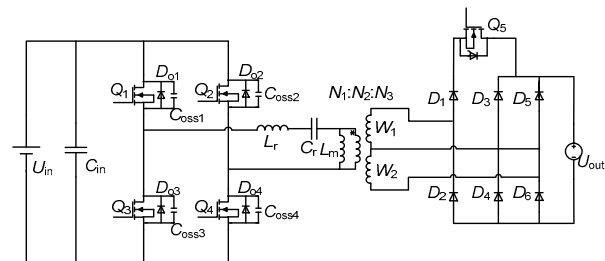


**Fig. 3 LLC resonant converters with a double-secondary transformer**

To overcome the shortcomings of a traditional LLC resonant converter, this paper adopts a variable-mode control strategy to gain higher efficiency for a wider range. In the so-called variable-mode control strategy, with no change in the structure of the circuit, the converter proactively controls the modes to shift it into a specific circuit formation and operating mode.

With the new variable-mode control strategy, different circuit modes can be adopted in accordance with different input voltages, and consequently, the range of input voltages can be widened, the MOSFET

operating frequency is reduced, the circuit design is facilitated, excitation loss and circuit loss are decreased, and efficiency is maximized.

## 2 Principles of variable-mode control strategy

Fig. 2 demonstrates the main circuit and MOSFETs of the full-bridge LLC resonant converter;  $Q_1$ – $Q_4$  are the inverter bridge arms. The diodes  $D_{01}$ – $D_{04}$  are parasitic diodes of  $Q_1$ – $Q_4$ , and  $C_{oss1}$ – $C_{oss4}$  are parasitic capacitances of  $Q_1$ – $Q_4$ . In the circuit for the primary winding of the transformer, the resonant capacitance  $C_r$ , resonant inductor  $L_r$ , and magnetic inductance  $L_m$  form a resonant tank. In the circuit for the secondary winding of the transformer, the diodes  $D_1$  and  $D_2$ , and the output capacitances  $C_{o1}$  and  $C_{o2}$ , form a voltage-doubling rectifier.

The variable-mode control strategy is composed of three operating modes as follows:

Mode 1: As shown in Fig. 4a, when the input voltage  $U_{in}$  is lower than a certain threshold  $U_{th1}$ , the circuit adopts a full-bridge LLC topology, and the converter works in variable-frequency mode. The circuit works at this moment in the mode of a traditional LLC resonant converter (Fig. 5a shows its main working waves), called ‘FB\_VF mode’.

Mode 2: As shown in Fig. 4b, when the input voltage is higher than the threshold value  $U_{th1}$  but lower than the threshold  $U_{th2}$ , the circuit adopts a full-bridge LLC topology, and the converter works in phase-shifting mode (Hamamura *et al.*, 2003; Lin *et al.*, 2013). Its main operating waveform is presented in Fig. 5b. The driving signal for  $Q_1$ – $Q_4$  here is the square signal with a 50% duty ratio, and  $Q_1$ – $Q_4$  are in phase-shifting control. At this point,  $Q_1$  and  $Q_3$  are the leading legs, and  $Q_2$  and  $Q_4$  are the lagging legs. The mode is called ‘FB\_PS mode’.

Mode 3: As shown in Fig. 4c, when the input voltage is higher than the threshold  $U_{th2}$  so that  $Q_2$  stays off while  $Q_4$  stays on,  $Q_1$  and  $Q_3$  are in variable-frequency control, and turn-ons and turn-offs are alternatively performed by the square signal with a 50% duty ratio. At this moment, the circuit shifts to a half-bridge LLC topology and the converter works in variable-frequency mode. With this mode, the DC gain is only half of that with Mode 1 under the same

working conditions. The operating waveform here is similar to Mode 1, called ‘HB\_VF mode’.

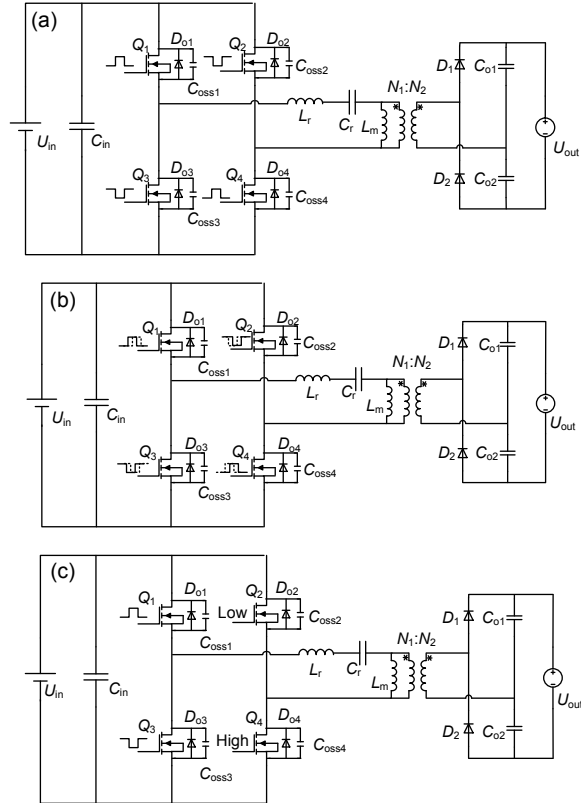


Fig. 4 Different operating modes: (a) Mode 1; (b) Mode 2; (c) Mode 3

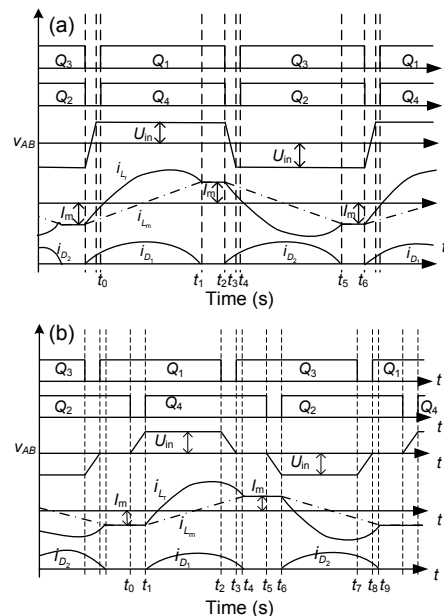


Fig. 5 Main waveforms of the LLC resonant converter in FB\_VF mode (a) and FB\_PS mode (b)

The principles of Mode 1 and Mode 3 were described in Liang et al. (2010). Hence, in this study we analyze only Mode 2 (FB\_PS mode) through examples, and suppose that the working frequency here is equal to or slightly higher than the resonant frequency.

1. In switch mode 0 (before  $t_0$ ) (Fig. 6a), before time  $t_0$ ,  $Q_1$  and  $Q_2$  are on,  $Q_3$  and  $Q_4$  are off,  $L_r$ ,  $C_r$ , and  $L_m$  resonate together. In the primary and secondary windings of the transformer flows there is no electronic current, and the converter load is powered by the output capacitances  $C_{o1}$  and  $C_{o2}$ .

2. In switch mode 1 ( $t_0-t_1$ ) (Fig. 6b),  $Q_2$  is turned off at time  $t_0$ : due to the buffering of the parasitic capacitances  $C_{oss2}$  and  $C_{oss4}$ ,  $Q_2$  could be turned off with zero voltage. Since this period is fairly short, it could likewise be considered that both the resonant current  $i_{L_r}$  and the magnetizing current  $i_{L_m}$  remain unchanged; thus, the converter load is still powered by the output capacitances  $C_{o1}$  and  $C_{o2}$ .

3. In switch mode 2 ( $t_1-t_2$ ) (Fig. 6c), at time  $t_1$ , the voltage of  $C_{oss2}$  rises to  $U_{in}$  while that of  $C_{oss4}$  is reduced to 0; the inverse-parallel diode  $D_{o4}$  is on, and hence  $Q_4$  could realize ZVS. At this moment, the voltages between points A and B are equal ( $u_{AB}=U_{in}$ ), the rectifier diode  $D_1$  turns on, the primary winding voltage is kept at  $nU_{out}$ , and the magnetizing current  $i_{L_m}$  increases linearly.

4. In switch mode 3 ( $t_2-t_3$ ) (Fig. 6d),  $Q_1$  is turned off at time  $t_2$ . Due to the buffering of  $C_{oss1}$ ,  $Q_1$  is turned on with zero voltage. The rectifier diode  $D_1$  is on,  $nU_{out}$  is added on  $L_m$ , and the magnetizing current  $i_{L_m}$  increases linearly.

5. In switch mode 4 ( $t_3-t_4$ ) (Fig. 6e), at time  $t_3$ , the voltage of  $C_{oss1}$  rises to  $U_{in}$  while that of  $C_{oss4}$  is reduced to 0, the inverse-parallel diode  $D_{o4}$  is on, and hence  $Q_3$  could realize ZVS. By this time,  $u_{AB}=0$ , the voltage of the transformer's primary winding is still clamped at  $nU_{out}$ , and  $i_{L_m}$  increases linearly.  $L_r$  and  $C_r$  resonate together.

6. In switch mode 5 ( $t_4-t_5$ ) (Fig. 6f), at time  $t_4$ ,  $i_{L_r}$  equals  $i_{L_m}$ , and the primary winding current  $i_{L_p}$  of the transformer is reduced to 0; the current in rectifier diode  $D_1$  naturally free-wheels to 0, and hence it can be turned off with zero voltage without a problem

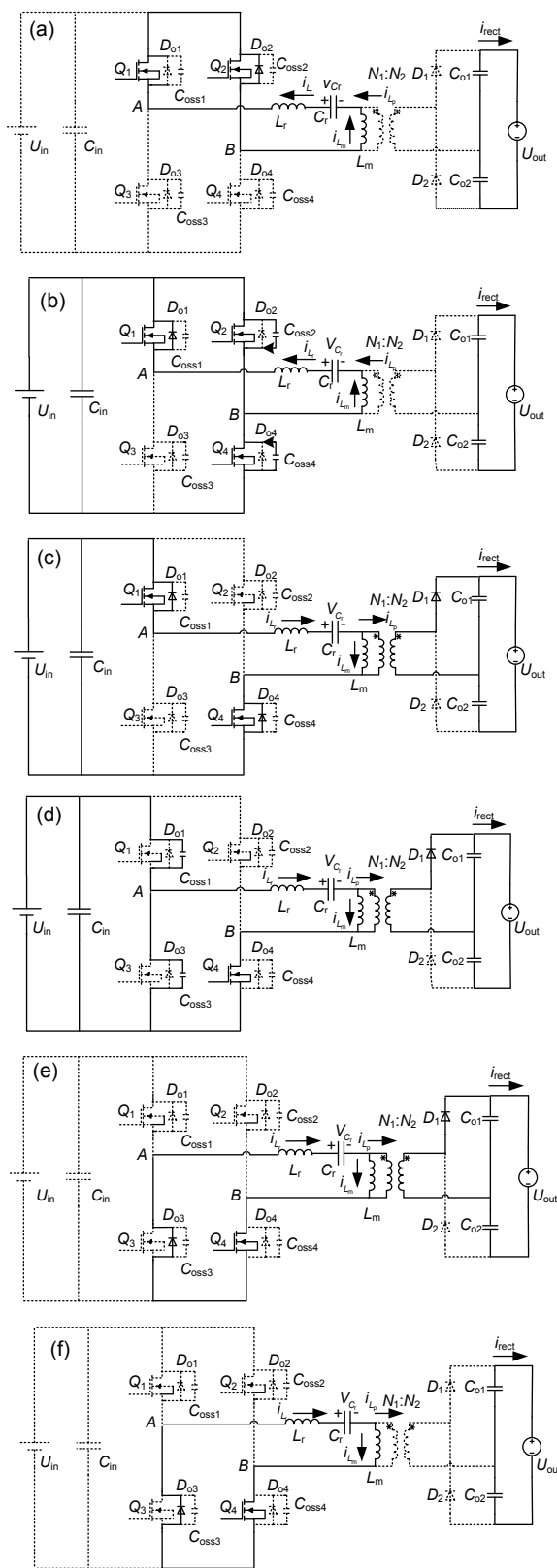


Fig. 6 Equivalent circuits in FB\_PS mode stages: (a) before  $t_0$ ; (b)  $t_0-t_1$ ; (c)  $t_1-t_2$ ; (d)  $t_2-t_3$ ; (e)  $t_3-t_4$ ; (f)  $t_4-t_5$

with reverse recovery. Load is powered by output capacitances  $C_{o1}$  and  $C_{o2}$ . In this period,  $L_r$  and  $L_m$  are connected in series and resonate with  $C_r$ .

At time  $t_5$ ,  $Q_4$  is turned off with zero voltage and another half operating period begins based on similar principles, which do not need to be repeated here.

Analyses of the working states and waveforms above indicate that zero-voltage switching of the primary winding MOSFET and zero-current switching of the secondary winding diode are realized on the circuit in FB\_PS mode.

### 3 Gain analysis of the LLC resonant converter in different modes

The resonant tank for the LLC resonant converter can be drawn similarly to the circuit diagram in Fig. 7, where  $R_{eq}=(8/\pi^2)n^2R_o$  ( $n=N_1/N_2$ ) is the load resistance converted to the primary winding.

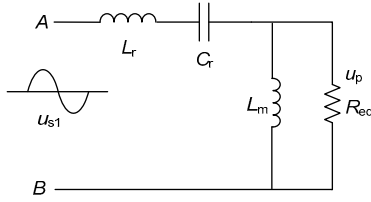


Fig. 7 A simplified equivalent circuit diagram of the LLC resonant converter resonant tank

From Fig. 7, the AC gain of the resonant tank is found to be approximate to

$$G(k_f, h, Q) = |u_p / u_{s1}| = \left[ \left( 1 + \frac{1}{h} - \frac{1}{k_f \cdot h^2} \right)^2 + Q^2 \cdot \left( k_f - \frac{1}{k_f} \right)^2 \right]^{\frac{1}{2}}, \quad (1)$$

where  $u_p$  denotes the RMS of the fundamental wave of the primary winding voltage's square wave,  $u_{s1}$  denotes the RMS of the fundamental wave of the resonant tank's input voltage,  $Q=Z_m/R_{eq}$  denotes the quality factor,  $h=L_m/L_r$  is the inductance ratio,  $k_f=f/f_r$  is the normalized frequency,  $f$  is the operating frequency,  $f_r=1/(2\pi\sqrt{L_r C_r})$  is the series resonant frequency, and  $Z_0=\sqrt{L_r/C_r}$  is the characteristic impedance.

As shown in Fig. 2, the output segment of the converter is the voltage-doubling rectifier. Thus, it is calculated to the secondary winding of the transformer,  $R_o=U_{out}^2/(4P_{out})$ , where  $U_{out}$ , which is a fixed constant, is the DC bus voltage that the resonant converter inputs into the inverter (the DC bus is directly connected with the inverter), and  $P_{out}$ , which changes with the working conditions, denotes the capacity of the grid-connected inverter. Hence, it can be concluded that the quality factor  $Q$  is a one-variable function of  $P_{out}$ . Assuming that the parameters of the LLC circuit are fixed,  $h$  and  $n$  are also constants.

Thus, the DC gain of the LLC resonant converter could approximately be expressed as

$$M(k_f, P_{out}) = U_{out}^2 / U_{in}. \quad (2)$$

#### 3.1 FB\_VF mode

When the input voltage  $U_{in}$  is lower than the threshold  $U_{th1}$ , and the main circuit is in FB\_VF mode, we have  $u_{s1}=\sqrt{2}U_{in}/\pi$ , while  $u_p=\sqrt{2}nU_{out}/(2\pi)$ , so the DC voltage gain could approximately be expressed as

$$M_{FB\_VF}(k_f, P_{out}) = \frac{U_{out}}{U_{in}} = \frac{2}{n} G(k_f, h, Q) = \frac{2}{n} \left[ \left( 1 + \frac{1}{h} - \frac{1}{k_f \cdot h^2} \right)^2 + \left( \frac{\pi^2 P_{out}}{2n^2 U_{out}^2} \sqrt{\frac{L_r}{C_r}} \right)^2 \cdot \left( k_f - \frac{1}{k_f} \right)^2 \right]^{\frac{1}{2}}. \quad (3)$$

It can be derived from Eq. (3) that the voltage transfer ratio  $M_{FB\_VF}$  is a function of  $k_f$  and  $P_{out}$ , and the 3D curves of  $M_{FB\_VF}$  with respect to  $k_f$  and  $P_{out}$  are shown in Fig. 8.

#### 3.2 FB\_PS mode

When the input voltage is higher than the threshold  $U_{th1}$ , and lower than threshold  $U_{th2}$ , the converter is in FB\_PS mode. Fig. 9 provides the driving waveforms of  $Q_1-Q_4$ , denoting a half period as  $\pi$ .  $\tau$  ( $0 \leq \tau \leq \pi$ ) is the phase shifting angle,  $u_{s1}=\sqrt{2}U_{in} \sin[(\pi-\tau)/2]/\pi$ , and  $u_p=\sqrt{2}nU_{out}/(2\pi)$ .

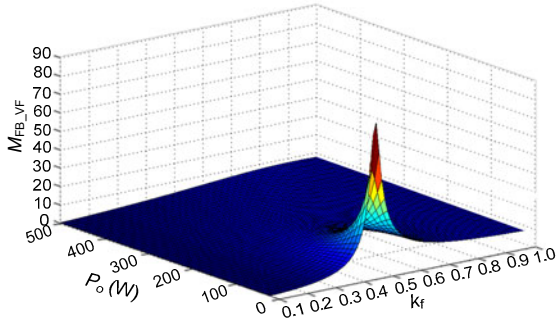


**Fig. 8** Three-dimensional curves of  $M_{FB\_VF}$  gain in FB\_VF mode

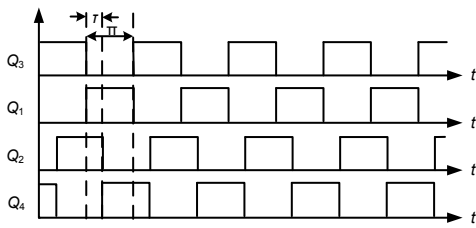


**Fig. 9** Driving waveforms in FB\_PS mode

During phase-shifting control, the converter operates around the resonant frequency; thus, the DC gain can approximately be expressed as

$$M_{FB\_PS}(k_f, P_{out}, \tau) = \frac{U_{out}}{U_{in}} = \frac{2 \sin[(\pi - \tau)/2]}{n} G(k_f, h, Q)$$

$$= \frac{2 \sin[(\pi - \tau)/2]}{n} \left[ \left( 1 + \frac{1}{h} - \frac{1}{k_f \cdot h^2} \right)^2 + \left( \frac{\pi^2 P_{out}}{2n^2 U_{out}^2} \sqrt{\frac{L_r}{C_r}} \right)^2 \right. \\ \left. \cdot \left( k_f - \frac{1}{k_f} \right)^2 \right]^{\frac{1}{2}}, \quad 0 \leq \tau \leq \pi. \tag{4}$$

From Eq. (4) it can be derived that the voltage gain ratio  $M_{FB\_PS}$  is a function of  $k_f$ ,  $P_{out}$ , and  $\tau$ . When the output power  $P_{out}$  and the frequency  $k_f$  stay unchanged, the gain will decrease with the rise of the phase shifting angle. Meanwhile, when the output power  $P_{out}$  and the phase shifting angle  $\tau$  stay unchanged, the gain is reduced with the increase in frequency. When  $P_{out}=300$  W, the 3D curves of  $M_{FB\_PS}$  with respect to  $k_f$  and  $\tau$  are shown in Fig. 10.

### 3.3 HB\_VF mode

When the input voltage is higher than the threshold  $U_{th2}$ , the circuit is in HB\_VF mode. As shown in Fig. 7, the input voltage  $u_{s1}$  of the RMS of the resonant tank in HB\_VF mode is half of that in

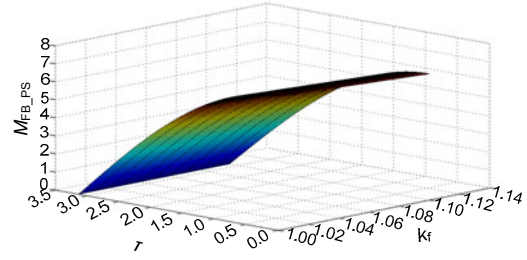


**Fig. 10** Three-dimensional curves for  $M_{FB\_PS}$  gain in FB\_PS mode

FB\_VF mode, where  $u_{s1} = \sqrt{2}U_{in}/(2\pi)$ . While  $u_p = \sqrt{2}nU_{out}/(2\pi)$ , the DC gain in FB-VF mode is half of that in HB\_VF mode, so the DC voltage gain could approximately be expressed as

$$M_{HB\_VF}(k_f, P_{out}) = \frac{U_{out}}{U_{in}} = \frac{1}{n} G(k_f, h, Q)$$

$$= \frac{1}{2} M_{FB\_VF}(k_f, P_{out})$$

$$= \frac{1}{n} \left[ \left( 1 + \frac{1}{h} - \frac{1}{k_f \cdot h^2} \right)^2 + \left( \frac{\pi^2 P_{out}}{2n^2 U_{out}^2} \sqrt{\frac{L_r}{C_r}} \right)^2 \right. \\ \left. \cdot \left( k_f - \frac{1}{k_f} \right)^2 \right]^{\frac{1}{2}}. \tag{5}$$

It can be derived from Eq. (5) that the voltage gain ratio  $M_{HB\_VF}$  is a function of  $k_f$  and  $P_{out}$ , and the 3D curves of  $M_{HB\_VF}$  with respect to  $k_f$  and  $P_{out}$  are shown in Fig. 11.

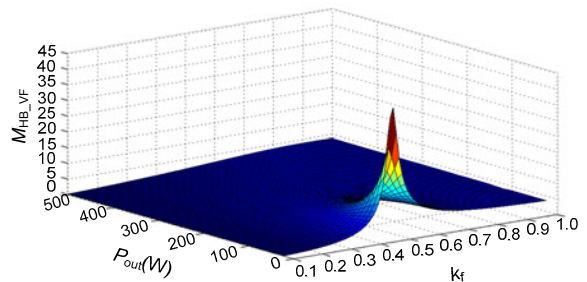


**Fig. 11** Three-dimensional curves of the  $M_{HB\_VF}$  gain in FB\_VF mode

When the circuit works in HB\_VF mode or FB\_VF mode, the working frequency  $f$  is normally subject to  $f_m < f < f_r$ , where  $f_m = (2\pi \sqrt{(L_r + L_m)C_r})^{-1}$  is another resonant frequency. If  $f \geq f_r$ , the ZCS of the secondary winding diode cannot be realized, and

hence the efficiency drops. When  $f_s \geq f_r$ , the circuit works in FB\_PS mode, the aforementioned problem can consequently be addressed, the input voltage range can be expanded, and a zero-current turn-off of the secondary winding diode can be realized.

#### 4 Parameter compatibility design for the variable-mode LLC resonant converter

The rated power equals  $P_{out}$ . Segment the circuit into three voltage sections. Presume that the operating voltage range in Mode 1 (FB\_VF mode) is  $U_{min1}-U_{max1}$  (Fig. 12), the circuit works under the maximum power point track (MPPT), and the output power rises with voltage. In Mode 2 (FB\_PS mode), the input voltage range is  $U_{min2}-U_{max2}$  and the output power remains  $P_{out}$ . In Mode 3 (HB\_VF mode), the input voltage range is  $U_{min3}-U_{max3}$  and the output power remains  $P_{out}$ .

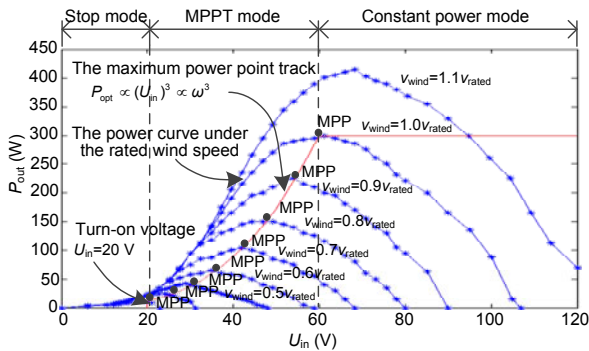


Fig. 12 Relationship between wind power turbine output voltage and output power

##### 4.1 Determination of the transformer turns ratio

When the voltage is within  $U_{min2}-U_{max2}$  or  $U_{min3}-U_{max3}$ , the output power  $P_{out}$  remains unchanged. Here, the corresponding voltage of the rated power  $P_{out}$  is  $U_{max2}$ , and  $U_{max2}=U_{min3}$ , with the resonance frequency  $f_r$ , and the dead time denoted as  $T_{dead}$ .

It is suggested that the voltage ratio between the primary and secondary sides of the transformer is

$$n = \frac{U_{out}/2}{U_{max2}}. \quad (6)$$

Thus, the transformer ratio is obtained.

##### 4.2 Calculation of magnetizing inductance $L_m$ , resonant inductor $L_r$ , and resonant capacitor $C_r$

In total, there are two conditions for ZVS on the primary side of the LLC resonant converter:

1. The current angle is greater than the dead angle. The dead angle refers to the product of dead time and the switch cycle angular frequency. The physical significance of a current angle greater than the dead angle lies in how the current on the resonant inductor during dead time cannot be reversed, ensuring that the parasitic diode being driven is kept open before the arrival of the driving signal; in other words, it is a soft switching.

2. Parasitic capacitance is fully charged or discharged during the dead time.

In Mode 1 (FB\_VF mode) (Fig. 12), the input voltage range is  $U_{min1}-U_{max1}$ , and the output power  $P_{out}$  is in direct proportion to the third power of the input voltage. Then, the minimal critical value of the current angle is  $\theta_{cri}=2\pi f_r \cdot T_{dead}$ , and the output power is  $P_{out} = kU_{in}^3 = k'f_s^3$ , where  $k$  and  $k'$  are constants. When the dead time is fixed, the realization of ZVS depends mainly on the magnetizing inductance  $L_m$ , operating frequency  $f_s$ , and output current  $I_o$  (with the output voltage  $U_{out}$  unchanged).

Based on the condition  $\theta_{cri} = 2\pi f_r \cdot T_{dead}$  and the current angle  $\theta \geq \theta_{cri}$ , we have

$$L_m \leq \frac{n^2 U_{out}/2}{2\pi f_r (2I_o) \tan(2\pi f_r T_{dead})} \cdot \frac{f_s}{f_r}. \quad (7)$$

Since the output voltage  $U_{out}$  does not change, we have  $I_o=P_{out}/U_{out}$ , and the output power is  $P_{out}=$

$$kU_{in}^3 = k'f_s^3, \text{ and } L_m \leq \frac{n^2 U_{out}^2}{8\pi f_r \tan(2\pi f_r T_d) \cdot k'f_s^2} \cdot \frac{1}{f_r}.$$

It is suggested that when operating frequency  $f_s$  grows,

$$\frac{n^2 U_{out}^2}{8\pi f_r \tan(2\pi f_r T_d) \cdot k'f_s^2} \cdot \frac{1}{f_r}$$

is reduced. Here, when the operating frequency  $f_s$  is at a maximum, i.e.,  $f_s=f_r$ , the minimum value of  $L_m$  can be obtained. This satisfies the ZVS condition of a primary MOSFET under the entire input voltage range of Mode 1 (FB\_VF mode).

In Mode 2 (FB\_PS mode) (Fig. 12), the input voltage range is  $U_{min2}-U_{max2}$ , the power is  $P_{out}$ ,

$$L_m \leq \frac{n^2 U_{out}/2}{2\pi f_r (2I_o) \tan(2\pi f_r T_d)} \cdot \frac{f_s}{f_r}, \text{ and the operating}$$

frequency rises with input voltage. Thus, as long as  $f_s=f_r$ ,  $L_m$  is kept at a minimum value. Similar results can be found for Mode 3 (HB\_VF mode).

Thus, when  $f_s=f_r$ ,  $L_m$  meets the ZVS conditions in a full range.

When the fully resonant point is set in advance, there are countless combinations of resonant inductor  $L_r$  and resonant capacitor  $C_r$ . We need to satisfy the requirements of fixed gain at the lowest operating frequency and  $L_r$  and  $C_r$  in conformity with the sum of the relevant output power. By using a fundamental harmonic approximation (FHA), the model can be built and the parameters are designed effectively.

In Mode 1 (FB\_VF mode), the operating frequency is below the resonance frequency  $f_r$ . From Fig. 12 it can be seen that the output power  $P_{out}$  is in direct proportion to the third power of the input voltage  $U_{in}$ , and  $P_{out} = kU_{in}^3$ .

Thus, the gain curve of the LLC resonant converter is found: when  $U_{in}=U_{min1}$ , the required gain, at maximum, is  $U_{out}/U_{min1}$ . Then, from the point of minimum input voltage, find the resonant inductor that satisfies the requirements for the maximum gain under the lowest frequency. Let the operating frequency under such a minimum input voltage be half of the resonance frequency.

When  $f_s=1/2f_r$ , i.e.,  $k_f=1/2$ , the equation can be written as

$$M_{FB\_VF}(k_f, P_{out}) = M_{FB\_VF}\left(\frac{1}{2}, kU_{min1}^3\right) \geq \frac{U_{out}}{U_{min1}}. \quad (8)$$

In Mode 2 (FB\_PS mode), the converter works above the resonance frequency  $f_r$ , the input voltage  $U_{in}$  grows, and the output power  $P_{out}$  remains unchanged. The converter here works under the conditions of fixed frequency and shifting phase, and the voltage is affected by both frequency and the duty ratio. When  $U_{in}=U_{min2}$ , the required gain is  $U_{out}/U_{min2}$  at maximum, where the operating frequency is  $f_r$  (i.e.,  $k_f=1$ ), the phase-shifting angle is 0, and the expression is

$$M_{FB\_PS}(k_f, P_{out}, \tau) = M_{FB\_PS}(1, P_{out}, 0) \geq \frac{U_{out}}{U_{min2}}. \quad (9)$$

In Mode 3 (HB\_VF mode), the converter works under resonance frequency  $f_r$  again, the input voltage  $U_{in}$  increases, and the output power  $P_{out}$  remains unchanged. Thus, the gain curve of the LLC resonant converter is found here. When  $U_{in}=U_{min3}$ , the required gain, to the maximum, is  $U_{out}/U_{min3}$ . Let the minimum operating frequency in Mode 3 be  $k_{HB\_VF\_min}$ . We have

$$M_{HB\_VF}(k_f, P_{out}) = M_{HB\_VF}(k_{HB\_VF\_min}, P_{out}) \geq \frac{U_{out}}{U_{min3}}. \quad (10)$$

When Eqs. (14)–(16) are satisfied, the optimized resonant inductor  $L_r$  and resonant capacitor  $C_r$  can be chosen.

To maintain the continuity of the input voltage change, we must keep the voltage gains between the mode shifting points at equality, i.e.,  $U_{max1}=U_{min2}$ ,  $U_{max2}=U_{min3}$ .

### 4.3 Criteria for selecting the voltage threshold between different modes

The common operating frequency  $f_s$  of the LLC resonant converter is subject to  $f_s \leq f_r$ , which is the condition under which the operation in Mode 1 (FB\_VF mode) is conducted.

When the operating frequency is  $f_s > f_r$ , the secondary diode of the transformer cannot be turned off with zero current (ZCS), resulting in lower efficiency. When the circuit works around the fully resonant point,  $f_s$  is slightly larger than  $f_r$ . Let  $T_s \approx T_r$  and the converter works in Mode 2 (FB\_PS mode).

A working analysis suggests that the LLC converter with PWM control can satisfy the circuit gain (enlarge the input voltage range) and meanwhile evade the problem that the secondary diode of the transformer cannot be turned off with zero current, thus having the shortcoming of frequency control in the region  $f_s > f_r$  under Mode 1. Specifically, the diode hard turn-off problem is accounted for.

In Mode 2 (FB\_PS mode), the gain of LLC is reduced with the duty ratio. When the phase-shifting angle grows, however, the magnetic inductor is clamped in a shorter time, the current at the intersection of resonance current and the magnetic current decreases, and thus it is harder to turn on the lagging leg with zero voltage.

While the duty ratio is changed, the features for pulse-frequency modulation (PFM) control are

retained and the gain reduces with the growth in frequency.

As depicted in Fig. 7, the input impedance of the resonant tank is given by

$$Z_{in} = \frac{1 - \omega^2 L_r C_r}{j\omega C_r} + \frac{j\omega L_m R_{eq}}{R_{eq} + j\omega L_m}, \quad (11)$$

where  $\omega = 2\pi f_s$ .

In Mode 2 (FB\_PS mode), the circuit represents the structure of the full-bridge resonant tank, and the current can be described as  $I_{r\_mode2} = U_{in}/Z_{in}$ .

In Mode 3 (HB\_VF mode), it is a half-bridge structure, and the equivalent input voltage is also a half of the full-bridge structure. Therefore, under the same operating frequency, the resonance current of Mode 3 (HB\_VF mode) is also a half of that of Mode 2 (FB\_PS mode),  $I_{r\_mode3} = U_{in}/(2Z_{in})$ .

From the shifting points equations between Mode 2 and Mode 3 in Table 1, we have

$$\begin{cases} \frac{U_{min3}}{Z_{in}} = \frac{U_{max2}}{2Z_{in}}, \\ M_{FB\_PS} = M_{HB\_VF} = \frac{U_{min3}}{U_{out}} = \frac{U_{max2}}{U_{out}}. \end{cases} \quad (12)$$

**Table 1 Mode shifting conditions**

Shifting type	Shifting point
From Mode 1 to Mode 2	$f_s = f_r$
From Mode 2 to Mode 3	$I_{r\_mode2} = I_{r\_mode3}$ $M_{FB\_PS} = M_{HB\_VF}$

The curves are shown in Fig. 13, which gives  $|1/Z_{in}|$ ,  $|1/(2Z_{in})|$ , and the operating frequency. Therefore, through comparing the resonant tank currents

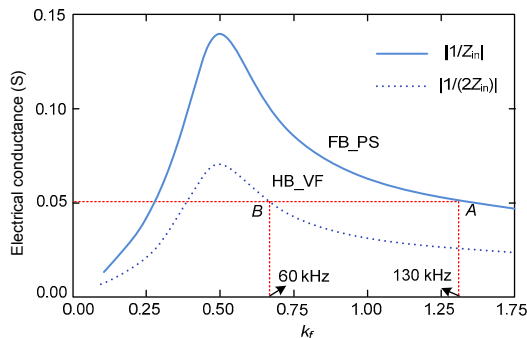


**Fig. 13 Comparison of resonant tank currents before and after mode shifting**

with the same input voltage and observing Eq. (12) and Fig. 13, for the voltage between the modes we have  $U_{th1} = U_{max1} = U_{min2}$  and  $U_{th2} = U_{max2} = U_{min3}$ .

Shifting from FB\_PS mode to HB\_VF mode (point A to B), it can be observed from Fig. 13 that when the gain  $U_{out}/U_{in}$  remains unchanged, the resonant tank current remains unchanged as well, and the operating frequency is reduced. As a result, the circuit works under  $f_s \leq f_r$ , the best condition, and vice versa.

### 5 Confirmation of circuit parameters and analysis of the modes

Based on the analysis and requirements presented above, we have the following calculations for the parameter design. Table 2 gives the known parameters calculated in Section 4.

**Table 2 Working parameters for the resonant converter and the parameters of other components**

Item	Value
Input voltage $U_{in}$	20–120 V
Output power $U_{out}$	450 V
Rated power $P_{out}$	300 W
Resonant frequency $f_r$	100 kHz
Resonant capacitor $C_r$	200 nF
Resonant inductor $L_r$	12.5 $\mu$ H
Excitation inductance $L_m$	45 $\mu$ H
MOSFET $Q_1-Q_4$	IPP65R310CFD
Rectifying diodes $D_1-D_2$	MUR8100
Ratio of transformer $N_1:N_2$	8:30

The input voltage range of the LLC converter is 20–120 V. At different input voltage levels, the converter works in a different mode.

According to the known conditions in Table 3, and with the method in Section 4.3, the voltage threshold can be calculated as  $U_{th1} = U_{max1} = U_{min2} = 60$  V and  $U_{th2} = U_{max2} = U_{min3} = 80$  V.

**Table 3 Relationship between the operating modes and input voltage**

Input voltage (V)	Operating mode	DC gain
20–60	FB_VF	22.500–7.500
60–80	FB_PS	7.500–5.625
80–120	HB_VF	5.625–3.750

It can be derived from Table 3 that when the input voltage range  $U_{in}$  is 20–60 V, the output voltage

$U_{out}$  is 450 V, DC gain  $M_{FB\_VF}$  is 22.500–7.500, and the converter works in FB\_VF mode. Fig. 12 indicates that when  $U_{in}$  is 20–60 V, the generator works on a maximum power tracking curve, as shown in Fig. 14, and the converter must work on the red curve among the 3D curves. As shown in Fig. 14, the working frequency and DC gain increase with an increase in the tracked power, where the tracking power  $P_{out}$  and input voltage  $U_{in}$  are in a third-order relationship.

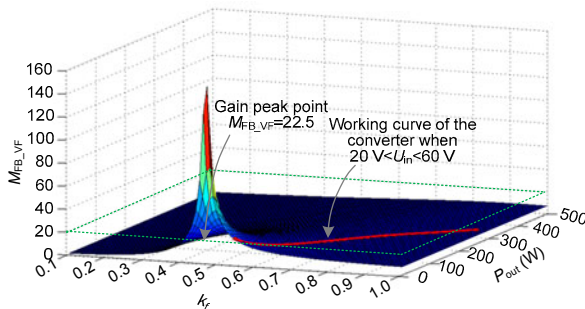


**Fig. 14 Working curves of the converter in FB\_VF mode (20 V <  $U_{in}$  < 60 V) (References to color refer to the online version of this figure)**

It can be derived from Table 1 that when the input voltage range  $U_{in}$  is 60–80 V, the DC gain  $M_{FB\_PS}$  is 7.500–5.625, and the converter works in FB\_PS mode. As shown in Fig. 12, when  $U_{in}$  is between 60 V and 80 V, the generator works in constant power mode, and  $P_{out}=300$  W. From Fig. 15 it can be derived that when  $P_{out}=300$  W and the phase shifting angle  $\tau$  stays unchanged, the gain  $M_{FB\_PS}$  drops with the reduction in phase shifting angle  $\tau$ ; furthermore, the  $M_{FB\_PS}$  gain drops with the decrease in working frequency  $k_f$ .

Theoretically, when the working frequency is the resonant frequency, the DC gain from 7.500 to 5.625 could be realized through a raise in the phase shifting angle  $\tau$ . The larger the phase shifting angle, however, the shorter the time for the excitation inductance to be voltage clamped, the smaller the current at the intersection point of the resonant current and magnetizing current, and the harder it is to realize the ZCS on the lagging bridge legs. Meanwhile, the resonant current rises, and the reactive power loss of the resonant tank grows. For these reasons, in FB\_PS mode, it is not recommended that the gain be obtained just by increasing the phase shifting angle. When the angle is too wide, ZVS cannot be realized, the circuit working efficiency is reduced, and a capacitive resonant tank

might occur, which leads to a short circuit on the bridge arms and causes damage.

Here is the solution. Since the  $M_{FB\_PS}$  gain drops with an increase in working frequency  $k_f$ , when the working frequency rises, the phase shifting angle  $\tau$  could be reduced, which shortens the time for the resonant current circulation and enhances the converter efficiency. From Fig. 15, it can be derived that when the range of the input voltage  $U_{in}$  is 60–80V, the working area can be divided into several parts. In each part’s control area, by fixing the frequency, the gain is reduced with the increase in the phase shifting angle. When it comes to the next part, as the working frequency increases, the phase shifting angle drops at first and then rises. By doing this, the phase shifting angle  $\tau$  in each part will not be too large, which ensures the ZCS of a secondary winding diode and the ZVS of a primary MOSFET.

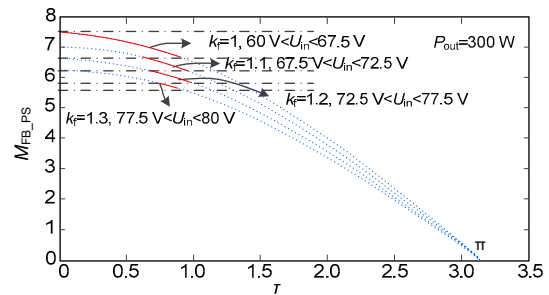


**Fig. 15 Working curves for the converter in FB\_PS mode (60 V <  $U_{in}$  < 80 V)**

It can be derived from Table 2 that when the input voltage range  $U_{in}$  is 80–120 V, the DC gain  $M_{FB\_PS}$  is 7.5–5.625, and the converter works in HB\_VF mode. As shown in Fig. 12, when  $U_{in}$  is between 80 and 120 V, the turbine works in constant power mode, and  $P_{out}=300$  W. From Fig. 16 it can be derived that when  $P_{out}=300$  W, the  $M_{HB\_VF}$  gain drops with a decrease in the working frequency  $k_f$ .

In Fig. 17, line  $AB$  represents the frequency-gain curve of FB\_VF mode. From  $A$  to  $B$ , the output power is also increasing. Line  $CD$  represents the phase shifting-gain curve, and the direction of the arrow indicates the direction along which the operating frequency increases. Fig. 17 shows that points  $B$  and  $C$  coincide. It means that the change of gain and control amount is continuous when shifting from FB\_VF mode to FB\_PS mode. When the input voltage is subject to  $U_{in} > U_{th1}=60$  V, as described in Table 1, the operating frequency  $f_s=f_r$ ; when it is shifted to

FB\_PS mode, the operating frequency remains unchanged. The phase-shifting angle  $\tau$  grows gradually as the voltage increases, until reaching the stable status. In contrast, when the input voltage is  $U_{in} < U_{th1} = 60$  V as described in Table 1 and the LLC is shifted to FB\_VF mode, the phase-shifting angle is reduced gradually to zero as the voltage decreases, and the switch frequency decreases and remains stable at  $f_s = f_r$ .

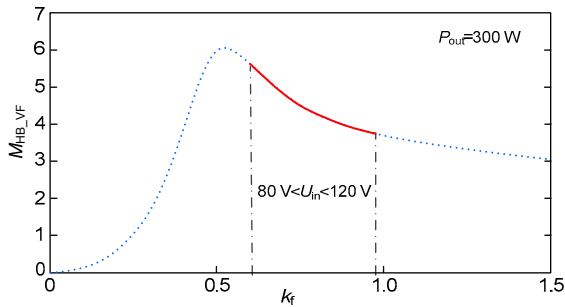


Fig. 16 Working curves for the converter in HB\_VF mode ( $80 \text{ V} < U_{in} < 120 \text{ V}$ )

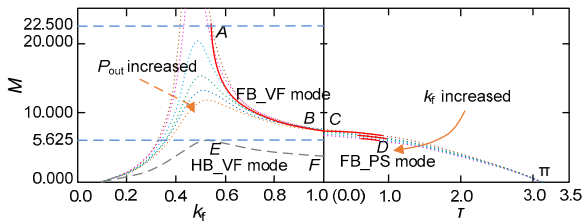


Fig. 17 Voltage gain variation curves for switching among three modes

In Fig. 17, line  $EF$  represents the frequency-gain curve of HB\_VF mode. From  $E$  to  $F$ , the output power remains unchanged. Fig. 17 shows that the operating frequency  $f_s$  and the phase-shifting angle  $\tau$  of points  $E$  and  $F$  are very different. It means that the change in the control amount is discontinuous when shifting from FB\_PS to HB\_VF. When the input voltage  $U_{in} > U_{th2} = 80$  V, the LLC is shifted to HB\_VF mode (shifted from  $D$  to  $E$ ), the phase-shifting angle is reduced to 0, and the operating frequency decreases. When the input voltage  $U_{in} < U_{th2} = 80$  V, the LLC is shifted to FB\_PS mode (shifted from  $E$  to  $F$ ), the phase-shifting angle grows, and the switch frequency augments to  $f_s = 1.3f_r$ .

## 6 Experimental verification

Fig. 18a presents waveforms of the resonant current, gate-source voltage  $U_{gs}$  of MOSFET  $Q_3$ ,

drain-source voltage  $U_{ds}$ , and output voltage  $U_{out}$ . When the LLC resonant converter works in FB\_VF mode, the input voltage  $U_{in} = 25$  V and output power  $P_{out} = 25$  W. From Fig. 18b it can be seen that when the circuit works in FB\_VF mode and with a light load on the primary winding MOSFET, ZVS can easily be realized.

Fig. 19a presents waveforms for the resonant current, gate-source voltage  $U_{gs}$  of MOSFET  $Q_3$ , drain-source voltage  $U_{ds}$ , and output voltage  $U_{out}$ . When the LLC resonant converter works in FB\_PS mode, the input voltage  $U_{in} = 65$  V and output power  $P_{out} = 300$  W. From Fig. 19b it can be seen that when the circuit works in FB\_PS mode and with a full load on the primary MOSFET, ZVS can also be realized easily.

Fig. 20a presents waveforms of resonant current, gate-source voltage  $U_{gs}$  of MOSFET  $Q_3$ , drain-source voltage  $U_{ds}$ , and output voltage  $U_{out}$ . When the LLC resonant converter works in FB\_VF mode, the input voltage  $U_{in} = 90$  V and output power  $P_{out} = 300$  W. From Fig. 20b it can be seen that when the circuit works in FB\_VF mode and with a full load on the primary winding MOSFET, the zero-voltage start can also easily be realized.

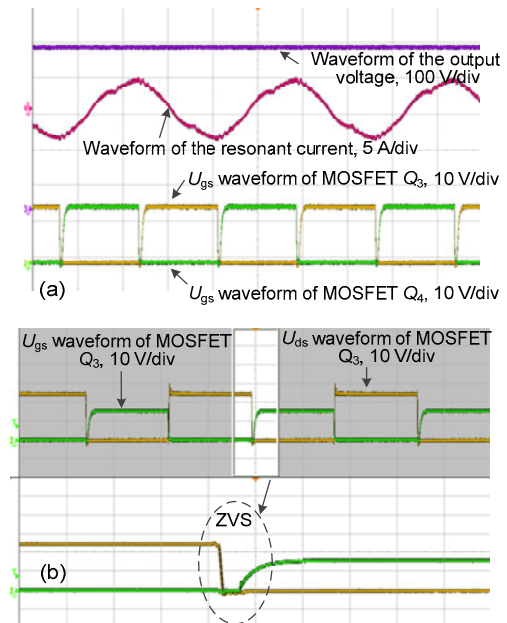
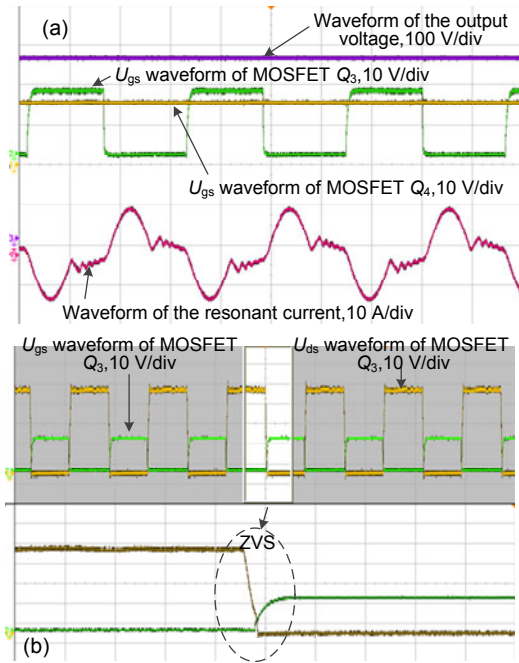
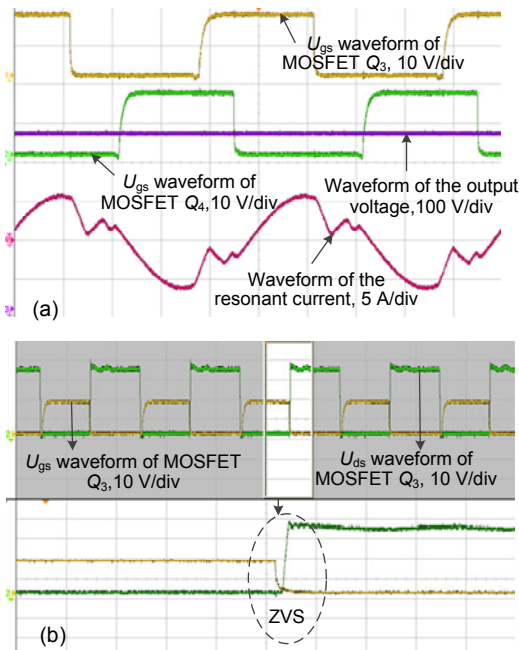


Fig. 18 FB\_VF mode of the LLC resonant converter: (a) waveforms of the resonant current and output voltage; (b) waveforms of  $U_{gs}$  and  $U_{ds}$  of the primary winding MOSFET (testing conditions:  $U_{in} = 25$  V,  $U_o = 450$  V, and  $P_{out} = 25$  W)



**Fig. 19** FB\_PS mode of the LLC resonant converter: (a) waveforms of resonant current and output voltage; (b) waveforms of  $U_{gs}$  and  $U_{ds}$  of the primary winding MOSFET (testing conditions:  $U_{in}=65$  V,  $U_o=450$  V, and  $P_{out}=300$  W)



**Fig. 20** HB\_VF mode of the LLC resonant converter: (a) waveforms of resonant current and output voltage; (b) waveforms of  $U_{gs}$  and  $U_{ds}$  of the primary winding MOSFET (testing conditions:  $U_{in}=90$  V,  $U_o=450$  V, and  $P_{out}=300$  W)

Fig. 21 presents the working efficiency curves of a resonant converter under the traditional full-bridge LLC strategy and the variable-mode control strategy. As shown in Fig. 21, the converter under the variable-mode control strategy has a 2% higher efficiency than the traditional one. Under the variable-mode control strategy, the maximum working efficiency can reach 95.7%.

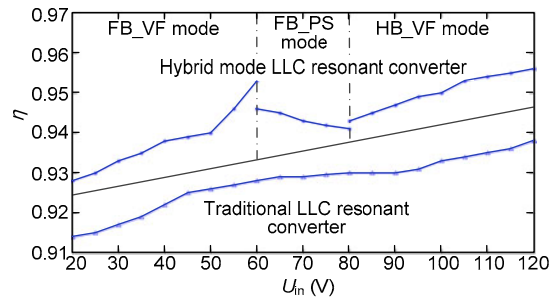


**Fig. 21** Efficiency curves for a resonant converter under traditional and the variable-mode strategies

## 7 Conclusions

Due to fluctuations in wind speed, wind power generation systems often face extremely wide input voltage ranges in the DC module. Given these circumstances, we proposed a new control strategy that enables the LLC resonant converter to work within an ultra-wide voltage range. When the input voltage is fairly low, an FB\_VF mode is adopted; when it rises to a certain extent, a full-bridge phase shifting mode (FB\_PS mode) is adopted; when it keeps rising, a half-bridge variable frequency mode (HB\_VF mode) is employed. By shifting between a half bridge and a full bridge, the input voltage range can be doubled. Furthermore, in the full-bridge phase shifting mode, the input voltage range can increase further. After experimental verification, it has been proven that the converter using the variable-mode control strategy has a higher efficiency than that using traditional strategies.

## References

Chen, W., Hong, X.Y., Wang, S.R., et al., 2010. High efficiency soft-switched step-up DC-DC converter with hybrid mode LLC+C resonant tank. 25th Annual IEEE Applied Power Electronics Conf. and Exposition, p.1358-1364. <http://dx.doi.org/10.1109/APEC.2010.5433406>

- Fang, X., Hu, H.B., Shen, J., et al., 2012. An optimal design of the LLC resonant converter based on peak gain estimation. 27th Annual IEEE Applied Power Electronics Conf. and Exposition, p.1286-1291.  
<http://dx.doi.org/10.1109/APEC.2012.6165984>
- Fang, Y., Xu, D.H., Zhang, Y.J., et al., 2007. Design of high power density LLC resonant converter with extra wide input range. 22nd Annual IEEE Applied Power Electronics Conf., p.976-981.  
<http://dx.doi.org/10.1109/APEX.2007.357633>
- Hamamura, S., Ninomiya, T., Yamamoto, M., et al., 2003. Combined PWM and PFM control for universal line voltage of a piezoelectric transformer off-line converter. *IEEE Trans. Power Electron.*, **18**(1):270-277.  
<http://dx.doi.org/10.1109/TPEL.2002.807177>
- Hu, J., Lin, H.P., Lu, Z.Y., et al., 2015. Flexible resonant tank for a combined converter to achieve an HPS and LED compatible driver. *Front. Inform. Technol. Electron. Eng.*, **16**(8):679-693.  
<http://dx.doi.org/10.1631/FITEE.1500054>
- Jang, J., Joung, M., Choi, B., et al., 2012. Dynamic analysis and control design of optocoupler-isolated LLC series resonant converters with wide input and load variations. *IET Power Electron.*, **5**(6):755-764.  
<http://dx.doi.org/10.1049/iet-pel.2011.0289>
- Jiang, Z.H., 2006. Power management of hybrid photovoltaic—fuel cell power systems. IEEE Power Engineering Society General Meeting, p.3458-3463.  
<http://dx.doi.org/10.1109/PES.2006.1709000>
- Jung, J.H., Kwon, J.G., 2007. Theoretical analysis and optimal design of LLC resonant converter. European Conf. on Power Electronics and Applications, p.1134-1143.  
<http://dx.doi.org/10.1109/EPE.2007.4417639>
- Liang, Z.G., Guo, R., Wang, G.Y., et al., 2010. A new wide input range high efficiency photovoltaic inverter. IEEE Energy Conversion Congress and Exposition, p.2937-2943. <http://dx.doi.org/10.1109/ECCE.2010.5618217>
- Lin, B.R., Nian, Y.B., Shiau, T.Y., 2013. Resonant converter with fixed frequency control. IEEE Region 10 Conf. TENCN, p.1-6.  
<http://dx.doi.org/10.1109/TENCON.2013.6718908>
- Rajaei, A., Mohamadian, M., Varjani, A.Y., 2013. Vienna-rectifier-based direct torque control of PMSG for wind energy application. *IEEE Trans. Ind. Electron.*, **60**(7): 2919-2929. <http://dx.doi.org/10.1109/TIE.2012.2227905>
- Steigerwald, R.L., 1988. A comparison of half-bridge resonant converter topologies. *IEEE Trans. Power Electron.*, **3**(2): 174-182. <http://dx.doi.org/10.1109/63.4347>
- Song, S.H., Kang, S.I., Hahm, N.K., 2003. Implementation and control of grid connected AC-DC-AC power converter for variable speed wind energy conversion systems. 18th Annual IEEE Applied Power Electronics Conf. and Exposition, p.154-158.  
<http://dx.doi.org/10.1109/APEC.2003.1179207>
- Tian, J., Su, C., Soltani, M., et al., 2014. Active power dispatch method for a wind farm central controller considering wake effect. 40th Annual Conf. of the IEEE Industrial Electronics Society, IECON, p.5450-5456.  
<http://dx.doi.org/10.1109/IECON.2014.7049333>
- Walker, G.R., Pierce, J.C., 2006. PhotoVoltaic DC-DC module integrated converter for novel cascaded and bypass grid connection topologies—design and optimisation. 37th IEEE Power Electronics Specialists Conf. Records, p.1767-1773.  
<http://dx.doi.org/10.1109/PESC.2006.1712242>
- Walker, G.R., Sernia, P.C., 2004. Cascaded DC-DC converter connection of photovoltaic modules. *IEEE Trans. Power Electron.*, **19**(4):1130-1139.  
<http://dx.doi.org/10.1109/TPEL.2004.830090>
- Wang, C.X., Lu, Z.X., Qiao, Y., 2013. A consideration of the wind power benefits in day-ahead scheduling of wind-coal intensive power systems. *IEEE Trans. Power Syst.*, **28**(1):236-245.  
<http://dx.doi.org/10.1109/TPWRS.2012.2205280>
- Yang, B., 2003. Topology Investigation of Front End DC/DC Converter for Distributed Power System. PhD Thesis, Virginia Polytechnic Institute and State University, Blacksburg, USA.
- Zhang, Z., Thomsen, O.C., Andersen, M.A.E., 2009. A DC-DC converter with wide input voltage range for fuel cell and supercapacitor application. Int. Conf. on Power Electronics and Drive Systems, p.1324-1329.  
<http://dx.doi.org/10.1109/PEDS.2009.5385904>